Luminescence properties of Eu2+-doped MAl2-xSixO4-xNx (M = Ca, Sr, Ba) conversion phosphor for white LED applications

Journal of The Electrochemical Society, **153** (4) G278-G282 (2006)
0013-4651/2006/153(4)/G278/5/$20.00 © The Electrochemical Society

Luminescence Properties of Eu^{2+}-Doped $MAl_{2-x}Si_xO_{4-x}N_x$ (M = Ca, Sr, Ba) Conversion Phosphor for White LED Applications

Y. Q. Li, G. de With, and H. T. Hintzen

Laboratory of Materials and Interface Chemistry, Department of Chemical Engineering and Chemistry, Eindhoven University of Technology, 5600 MB, Eindhoven, The Netherlands

Undoped and Eu-doped $MAl_{2-x}Si_xO_{4-x}N_x$ (M = Ca, Sr, Ba) were synthesized by a solid-state reaction method at 1300–1400°C under nitrogen–hydrogen atmosphere. The solubility of $(SiN)^+$ in MAl_2O_4 was determined. Nitrogen can be incorporated into MAl_2O_4 by replacement of $(AlO)^+$ by $(SiN)^+$, whose amount of solubility depends on the M cation. The solubility of $(SiN)^+$ is very low in $CaAl_2O_4$ and $SrAl_2O_4$ lattices ($x \approx 0.025$ and 0.045, respectively), whereas a large amount of $(SiN)^+$ can be incorporated into $BaAl_2O_4$ ($x \approx 0.6$). Incorporation of $(SiN)^+$ hardly modifies the luminescence properties of Eu^{2+}-doped MAl_2O_4 (M = Ca, Sr) because of limited solubility of $(SiN)^+$, showing the blue and green emission at almost constant wavelength of 440 and 515 nm, respectively. Eu^{2+}-doped $BaAl_{2-x}Si_xO_{4-x}N_x$ exhibits a broad green emission band with a maximum in the range of 500–526 nm, depending on the concentration of $(SiN)^+$ and Eu^{2+}. In addition, both excitation and emission bands of Eu^{2+} show a significant red shift as nitrogen is incorporated. $BaAl_{2-x}Si_xO_{4-x}N_x$:Eu^{2+} can be efficiently excited in the range of 390–440 nm radiation, which makes this material attractive as conversion phosphor for white light-emitting diode (LED) lighting applications.
 [DOI: 10.1149/1.2167950]

Manuscript submitted June 7, 2005; revised manuscript received September 1, 2005. Available electronically February 13, 2006.

As an important class of phosphors, Eu^{2+}-doped MAl_2O_4 (M = Ca, Sr, Ba), has been widely used as persistent luminescent materials because of their high efficiency, chemical stability, and long-lasting high-luminance afterglow characteristics.[1-3] These phosphors also have been proposed for plasma display panel (PDP)[4] and optoelectronic applications.[5] Under ultraviolet and cathode-ray excitation these phosphors show a strong blue (M = Ca), green (M = Sr), and blue-green (M = Ba) fluorescence.

In MAl_2O_4 (M = Ca, Sr, Ba), the three-dimensional framework is built-up by a motif of six rings formed by corner-sharing AlO_4 tetrahedra. The tetrahedral framework is isostructural, with the SiO_2 polymorph having the tridymite structure.[6-8] The various MAl_2O_4 structures differ in the arrangement and number of crystallographic sites of the divalent cations within the channels formed by the AlO_4 rings. $CaAl_2O_4$ has a monoclinic structure in space group $P2_1/n$. In this structure there are three Ca sites: two of them are sixfold and the third is ninefold coordinated, with the oxygen atoms in a different channel. However, for the larger M cations, $SrAl_2O_4$ and $BaAl_2O_4$ crystallize in a monoclinic and a hexagonal system with the space group $P2_1$ and $P6_3$, respectively. Both Sr and Ba ions occupy two crystallographic sites, which are located in the channels of the AlO_4 rings, each with ninefold coordination with the oxygen anions.

Although extensive investigations have been done on Eu^{2+}-doped alkaline earth aluminates MAl_2O_4 (M = Ca, Sr, Ba),[9-15] in previous studies considerable attention has been paid to improve the performance of these phosphors by partial substitution of the M ion (for example, replacement of Ca with Sr and vice versa[10,11]) and the Al ion (i.e., partial replacement of Al by B[12]), and/or by codoping activator ions (for example, Eu^{2+} with Dy^{3+}).[15] These effects can enhance the efficiency, optimize emission color range, and extend persistence time. However, it is only possible to tailor the excitation and absorption bands in the UV range. As a consequence, for obtaining an efficient emission these phosphor materials have to be excited in the UV region (e.g., below 350 nm). Therefore, with respect to white light-emitting diode (LED) applications, the excitation bands of Eu^{2+}-doped MAl_2O_4 (M = Ca, Sr, Ba) phosphors do not match with the UV-blue emission (~370–460 nm) from InGaN-based LEDs. For use as wavelength conversion phosphors for white-light LEDs, usually a strong absorption in the UV-blue range (i.e., 370–460 nm) and highly efficient conversion from absorbed blue into green, yellow, and red light are required.[16] Hence, in order to make MAl_2O_4:Eu^{2+} (M = Ca, Sr, Ba) phosphors meet these requirements, apart from the above-mentioned routes other novel approaches have to be adopted. Recently, Eu^{2+}-doped alkaline-earth-silicon-nitride[17,18] and oxynitride[19] have shown an unusual long wavelength emission with excitation in the visible range (370–460 nm). Therefore, if silicon and nitrogen atoms can be incorporated into MAl_2O_4, e.g., $(AlO)^+$ replacement by $(SiN)^+$ [which is an opposite routine to convert nitride into oxynitride, for example, $(SiN)^+ \rightarrow (AlO)^+$ replacement in $Si_3N_4 \rightarrow SiAlON$[20] and $Y_2Si_3O_3N_3 \rightarrow Y_2Si_{3-x}Al_xO_{3+x}N_{4-x}$[21]], it is expected that $MAl_{2-x}Si_xO_{4-x}N_x$:Eu^{2+} will extend the excitation bands into the visible range and emit at longer wavelengths, i.e., green and yellow emission, due to the oxide conversion into oxynitride lattice. Such a modification of the framework of MAl_2O_4:Eu^{2+} (M = Ca, Sr, Ba) has already proved an efficient approach to improve its luminescence for white-light LED applications.[22]

In this work, we synthesized undoped and Eu^{2+}-doped $MAl_{2-x}Si_xO_{4-x}N_x$ ($0 \leqslant x < 2$, M = Ca, Sr, Ba) materials by a solid-state reaction and investigated the existence region of $MAl_{2-x}Si_xO_{4-x}N_x$ compounds with the stuffed tridymite structure. The effect of the substitution of $(SiN)^+$ for $(AlO)^+$ on the phase formation and crystal structure was studied by X-ray powder diffraction combined with Rietveld refinement. Finally, the luminescence of Eu^{2+}-doped $MAl_{2-x}Si_xO_{4-x}N_x$ (M = Ca, Sr, Ba) and the dependence of luminescence properties on Eu^{2+} concentration in $BaAl_{2-x}Si_xO_{4-x}N_x$ were also investigated.

Experimental

Starting materials.— MCO_3 (M=Ca, Sr, Ba) (Merck, >99.0%), SiO_2 (Degussa Aerosil OX50), γ-Al_2O_3 (AKPG, >99.995), α-Si_3N_4 (SKW Trostberg, α content 23.3%, O content 0.7 wt %) and Eu_2O_3 (Rhône-Poulenc, 99.99%) were employed as the raw materials. Oxygen presence in the Si_3N_4 starting powder was not considered in the synthesis procedures.

Synthesis of undoped and Eu^{2+}-doped $MAl_{2-x}Si_xO_{4-x}N_x$ (M = Ca, Sr, Ba).— Si_3N_4 was used as the source of $(SiN)^+$ using the following reaction

$$MCO_3 + (2-x)/2Al_2O_3 + x/4Si_3N_4 + x/4SiO_2 \rightarrow MAl_{2-x}Si_xO_{4-x}N_x + CO_2 \quad [1]$$

The raw materials were homogeneously wet-mixed in the appropriate amounts by a planetary ball mill for 4–5 h in isopropanol with

agate balls in an agate container. After mixing the mixture was dried in a stove and ground in an agate mortar. Subsequently, the powders were fired in Mo or alumina crucibles at 1300–1400°C for 8–12 h in a reducing atmosphere of N_2–H_2 (10%) in a horizontal tube furnace two times with an intermediate grinding between the firing steps. The same processes were adopted for obtaining Eu-doped materials.

Characterization.— The obtained samples were analyzed by X-ray powder diffraction on a Rigaku D/Max-γB diffractometer operating at 40 kV, 30 mA with Bragg–Brentano geometry (flat graphite monochromator, scintillation counter) using Cu Kα radiation. Phase formation was checked by a routine scan (2°/min). The lattice parameters were determined in the 2θ range of 10–90° with a step-scan mode using silicon powder as an internal standard with a step size of 0.01° 2θ and a counting time of 6 s per step. In order to correlate the changes of the local structures with the luminescence properties, the structure of $BaAl_{2-x}Si_xO_{4-x}N_x$ was refined by the Rietveld method[23] using structural parameters of $BaAl_2O_4$[8] as the starting model, assuming both Si^{4+} and N^{3-} random distributing over the Al^{3+} and O^{2-} sites, respectively, in $BaAl_2O_4$. For the Rietveld refinement XRD data were recorded with a step-scan mode within a 2θ range of 10–120° with a step size of 0.01° 2θ and a counting time of 15 s per step. The Rietveld refinement was performed using the program GSAS.[24,25] The refined parameters include the scale factor, zero shift, background, lattice parameters, peak profile parameters, fractional coordinates of individual atoms, and isotropic displacement parameters.

The photoluminescence spectra were determined at room temperature on the powder samples by a Perkin-Elmer LS-50B luminescence spectrometer with a Xenon discharge lamp as excitation source. The radiation was detected by a red sensitive photomultiplier R928. The spectra were obtained in the range of 200–700 nm with a scanning speed of 100 nm/min and excitation and emission slit widths of 2.5 nm. Excitation spectra were automatically corrected for the variation in the lamp intensity by a second photomultiplier and a beam splitter, and all the emission spectra were corrected by taking into account the combined effect of the spectral response of the R928 detector and the monochromator by using the measured spectra of a calibrated W-lamp as the light source. Diffuse reflectance spectra were recorded in the range of 230–700 nm, with $BaSO_4$ white powder (~100%) and black felt (3%) as the references.

Results and Discussion

Effect of $(SiN)^+$ substitution for $(AlO)^+$ in MAl_2O_4 (M = Ca, Sr, Ba) on phase formation and structure.— When nitrogen is incorporated in MAl_2O_4, $(AlO)^+$ is expected to be replaced by the $(SiN)^+$ pair to form hybrid (Al,Si)–$(O,N)_4$ tetrahedra in the framework. As proof, the lattice parameters are expected to decrease, corresponding to the unit cell volume shrinkage because of shorter Si–$N^{[2]}$ distances (~1.65 to 1.75 Å,[26] $N^{[2]}$ denotes nitrogen bridging two silicon atoms) as compared to the Al–$O^{[2]}$ distances (~1.70 to 1.78 Å,[27-29] $O^{[2]}$ denotes the oxygen bridging two aluminum atoms) in MAl_2O_4. With the ionic radius of M decreasing from Ba to Ca, it is found that the incorporation of nitrogen according to Reaction 1 becomes more difficult. As a consequence, the maximum solubility of $(SiN)^+$ in MAl_2O_4 significantly decreases from Ba to Sr and Ca compounds. In the case of $CaAl_2O_4$ and $SrAl_2O_4$, the solubility of $(SiN)^+$ is almost negligible. The obtained lattice parameters of $MAl_{2-x}Si_xO_{4-x}N_x$ as a function of x demonstrate that the maximum solubility of $(SiN)^+$ in $CaAl_2O_4$ and $SrAl_2O_4$ lattice is only $x \approx 0.025$ (i.e., 1.25 mol %) and $x \approx 0.045$ (i.e., 2.25 mol %), respectively (Fig. 1). Accordingly, when the x value surpasses the maximum solubility, a secondary phase of $Ca_2Al_2SiO_7$ or $Sr_2Al_2SiO_7$ appears in the $CaAl_{2-x}Si_xO_{4-x}N_x$ and $SrAl_{2-x}Si_xO_{4-x}N_x$ system, respectively.

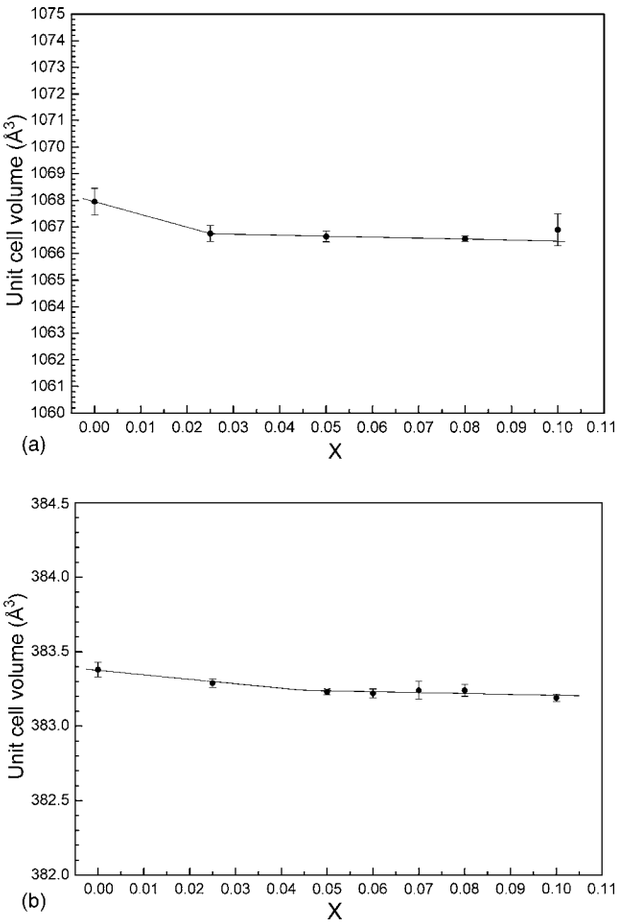

Figure 1. Relationship between the unit cell volume and x values of (a) $CaAl_{2-x}Si_xO_{4-x}N_x$ and (b) $SrAl_{2-x}Si_xO_{4-x}N_x$.

In contrast, the lattice parameters and in particular the unit cell volume of $BaAl_{2-x}Si_xO_{4-x}N_x$ significantly decrease with increasing x value up to 0.6, indicating that $(SiN)^+$ is effectively incorporated into $BaAl_2O_4$ lattice to a high extent (Fig. 2). For x values larger than 0.6, the unit cell volume remains almost constant and a distinct secondary phase of Ba_2SiO_4 is found; thus, the maximum solubility

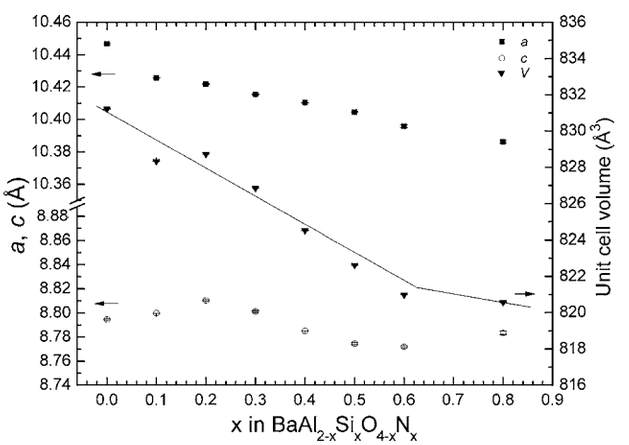

Figure 2. Relationship between the lattice parameters of $BaAl_{2-x}Si_xO_{4-x}N_x$ and x.

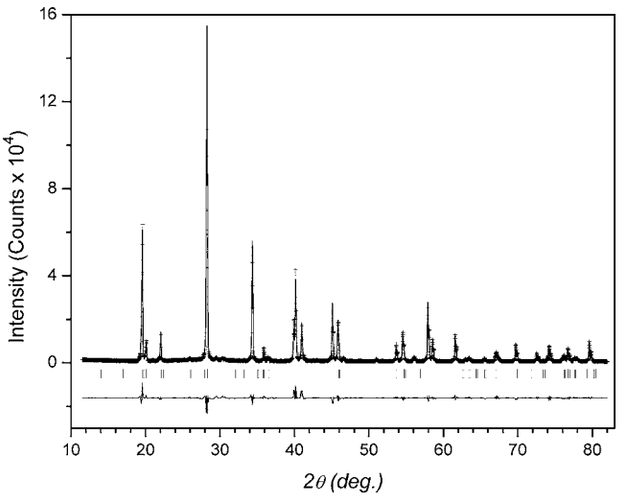

Figure 3. XRD pattern for $BaAl_{2-x}Si_xO_{4-x}N_x$ ($x = 0.3$). Plus marks (+) represent the observed intensities, and the solid line is the calculated pattern. A difference (obs.–calc.) plot is shown in the bottom. The bars above the difference profile indicate the positions of Bragg reflections for $BaAl_2O_4$ with the tridymite structure.

of $(SiN)^+$ in $BaAl_2O_4$ is about $x = 0.6$ (Fig. 2). Consequently, the observed X-ray diffraction (XRD) pattern of $BaAl_{2-x}Si_xO_{4-x}N_x$ perfectly matches with the calculated pattern based on $BaAl_2O_4$ tridymite structure[8] (Fig. 3). Although, as expected, both the *a* and *c* axes decrease with increasing *x* [i.e., $(SiN)^+$ content, Fig. 2], the *c*/*a* ratio of $BaAl_{2-x}Si_xO_{4-x}N_x$ is almost constant ($\sim$0.843).

The larger solubility of $(SiN)^+$ in the $BaAl_2O_4$ lattice may be related to the larger difference between the shortest (1.665 Å) and longest (1.808 Å) Al–O bonds of the Al_2O_4 network (reflected by the large standard deviation of 0.042 Å for the Al–O distances) as induced by the larger ionic size of the Ba ion. These largely distorted (AlO_4) tetrahedra are probably very well compatible with incorporation of a Si–N pair without changing its structure too much. In contrast, in $CaAl_2O_4$ and $SrAl_2O_4$ all the tetrahedral (AlO_4) units are very regular (i.e., the Al–O distances are very similar, with a very small standard deviation of 0.012 and 0.013 Å for the Ca and Sr compound, respectively[6,7]), resulting in strong distortions due to incorporation of SiN.

When $(AlO)^+$ is replaced by $(SiN)^+$ in $BaAl_2O_4$, the average (Si,Al)–(O,N) distances, obtained by the Rietveld refinement, decrease for larger $(SiN)^+$ amounts corresponding to an overall shrinkage of the lattice. For example, these average (Si,Al)–(O,N) distances are 1.7534, 1.7529, and 1.7431 Å, respectively, for $x = 0$, 0.1, and 0.3 in $BaAl_{2-x}Si_xO_{4-x}N_x$. At the same time, however, the average Ba–(O, N) distances slightly increase (i.e., 2.918 Å vs 2.924 Å for $x = 0$ and 0.3, respectively), indicating that Ba needs more space due to coordination with N (larger than O). It is worth noting that for a better understanding of the site preferences of Si (on the four available Al sites) and N (on the six available O sites) in $BaAl_2O_4$, neutron diffraction experiments need to be performed due to the similar scattering factors of N^{3-}/O^{2-} and Al^{3+}/Si^{4+} for X-ray powder diffraction.

Luminescence properties of Eu-doped $MAl_{2-x}Si_xO_{4-x}N_x$ (M = Ca, Sr, Ba).— The luminescence properties of Eu-doped $MAl_{2-x}Si_xO_{4-x}N_x$ strongly depend on the types of the cation M, similar to the case of $MAl_2O_4:Eu^{2+}$ (M = Ca,Sr,Ba).[9-15] While the position of the Eu^{2+} excitation and emission bands is nearly independent of *x* for M=Ca and Sr, it strongly depends on *x* for M = Ba. Overview results of the obtained luminescence properties (i.e., excitation, emission, and Stokes shift) are listed in Table I.

$MAl_{2-x}Si_xO_{4-x}N_x:Eu^{2+}$ (M = Ca, Sr).— As described above, the solubility of $(SiN)^+$ in $CaAl_{2-x}Si_xO_{4-x}N_x$ and $SrAl_{2-x}Si_xO_{4-x}N_x$ is very low (Table I); hence, it is expected that the excitation and emission spectra of the Eu-doped compounds have no significant change compared with those of Eu-doped MAl_2O_4 (M = Ca, Sr). Both the excitation and emission behaviors are very similar, except for some minor differences like an enhanced shoulder at about 370 nm in the excitation spectrum for M = Ca and a slightly broadened excitation band for M = Sr. Additionally, the maximal shift of the Eu^{2+} emission bands is less than 10 nm with increasing *x* (Fig. 4). These observations are consistent with the above-mentioned conclusion that the solubility of $(SiN)^+$ in $MAl_{2-x}Si_xO_{4-x}N_x$ (M = Ca, Sr) is negligible, and consequently, such limited $(SiN)^+$ incorporation does hardly modify the local coordination of the Eu^{2+} (Ca or Sr) ions.

$BaAl_{2-x}Si_xO_{4-x}N_x:Eu^{2+}$.— With the content of incorporated $(SiN)^+$ increasing, an additional excitation band appears for $BaAl_{2-x}Si_xO_{4-x}N_x:Eu^{2+}$ (10 mol %), peaking at 425–440 nm for *x* values above 0.3 (Fig. 5). Correspondingly, the broad emission band shifts to a longer wavelength from 498 to 527 nm up to $x = 0.6$ (Fig. 5), which is also consistent with our observation of a high solubility of $(SiN)^+$ in $BaAl_2O_4$ (Table I and Fig. 2). Because the $BaAl_2O_4$ lattice becomes more rigid when more covalent nitrogen is introduced in the three-dimensional $(Al,Si)(O,N)_4$ framework, it is evident that the Stokes shift shows a decrease in the *x* range from 0 to 0.3 (Table I). Therefore, we can readily attribute the red shift of

Table I. Overview of structural parameters of undoped and luminescence data of 10 mol % Eu-doped $MAl_{2-x}Si_xO_{4-x}N_x$ (M = Ca, Sr, Ba).

$MAl_{2-x}Si_xO_{4-x}N_x$	M = Ca		M = Sr		M = Ba	
Maximum solubility of $(SiN)^+$	$x = 0.025$		$x = 0.045$		$x = 0.6$	
Structural parameters	Monoclinic $P2_1/n$		Monoclinic $P2_1$		Hexagonal $P6_3$	
x	$x = 0$	$x = 0.02$	$x = 0$	$x = 0.02$	$x = 0$	$x = 0.3$
a (Å)	8.6808(3)	8.6714(4)	8.4435(8)	8.4384(10)	10.4468(6)	10.4454(3)
b (Å)	8.0928(4)	8.0923(7)	8.8184(9)	8.8275(8)		
c (Å)	15.1950(8)	15.1979(3)	5.1575(7)	5.1527(5)	8.7946(5)	8.8012(7)
β (°)	90.26(1)	90.28(1)	93.40(1)	93.32(2)		
V (Å^3)	1067.47(8)	1066.45(6)	383.35(10)	383.18(9)	831.22(8)	826.85(8)
Excitation band (nm)	260, 329, 380	260, 339, 380	260, 340, 386, 420	260, 340, 386, 420	280, 340, 387	280, 340, 400, 440
Emission band (nm)	438	443	514	519	498	526
Stokes shift (cm^{-1})[a]	3500	3600	6500	6600	5800	3700
Crystal field splitting (cm^{-1})[b]	13,360	13,600	14,000	14,000	10,000	13,000

[a] Stokes shift calculated from the energy difference between the lowest 5d excitation band and emission band of Eu^{2+}.
[b] Crystal-field splitting estimated from the energy difference between highest and lowest observed 5d excitation levels of Eu^{2+}

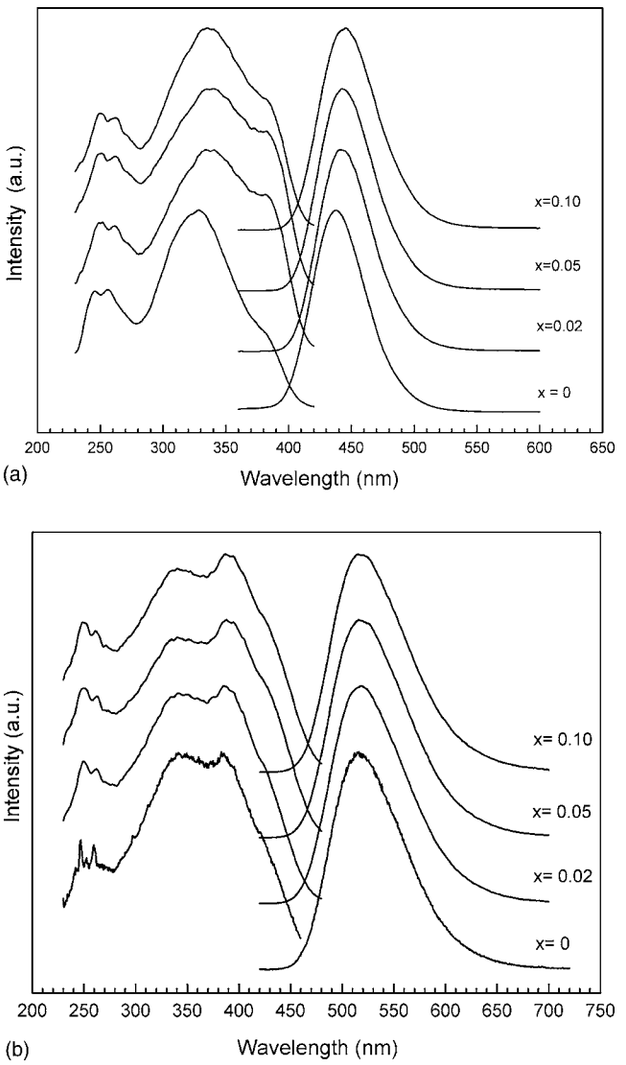

Figure 4. Excitation (left) and emission (right) spectra of $MAl_{2-x}Si_xO_{4-x}N_x$:Eu (10%) with various x: (a) M = Ca (λ_{exc} = 340 nm; λ_{em} = 450 nm); (b) M = Sr (λ_{exc} = 387 nm; λ_{em} = 520 nm).

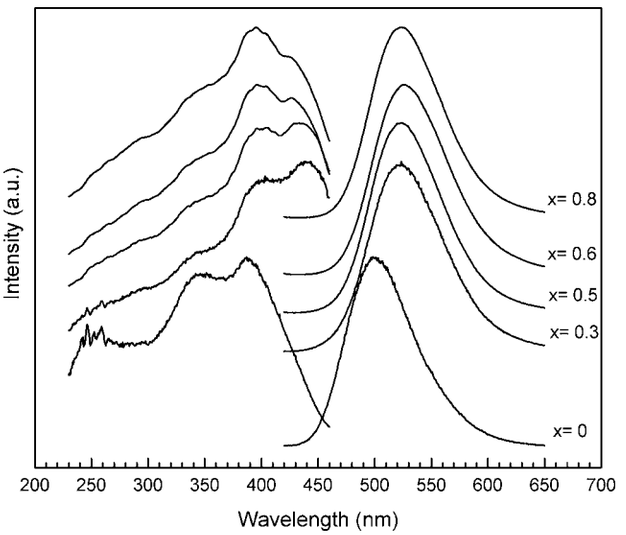

Figure 5. Excitation (left) and emission (right) spectra of $BaAl_{2-x}Si_xO_{4-x}N_x$:Eu (10%) with various x (λ_{exc} = 390 nm, λ_{em} = 500 nm, for x = 0; and λ_{exc} = 440 nm, λ_{em} = 530 nm for x = 0.3–0.8).

the Eu^{2+} emission band to a concomitant shift of the lowest excitation band due to an increase of the crystal field splitting of the 5d state of the Eu^{2+} ions as a consequence of the replacement of O^{2-} by N^{3-}. Also, an increase of degree of covalent bonding induced by nitrogen contributes to this shift (Table I). For $x > 0.3$, the excitation bands show a slight blue-shift, especially for $x > 0.5$ (Fig. 5), which can be understood from the fact that the Eu_{Ba}–O/N distances become larger as the amount of $(SiN)^+$ increases, resulting in a smaller crystal field splitting and counteracting the effect of the replacement of O^{2-} by N^{3-}. The integrated emission intensity of $BaAl_{2-x}Si_xO_{4-x}N_x$:Eu (10 mol %) reaches a maximum at x = 0.3 for excitation in the range of 400–460 nm. When x is larger than 0.3, the emission intensity shows a significant decrease. The quantum efficiency of $BaAl_{2-x}Si_xO_{4-x}N_x$:Eu (10 mol %, x = 0.3) is about 54%, with an excitation wavelength at 460 nm.

Besides the replacement of $(AlO)^+$ by $(SiN)^+$, as usual the Eu^{2+} concentration also shows a significant influence on the structure and luminescence properties of $BaAl_{2-x}Si_xO_{4-x}N_x$:Eu^{2+}. Figure 6 shows the lattice parameter changes of $BaAl_{2-x}Si_xO_{4-x}N_x$ (x = 0.3) as a function of the Eu concentration. As expected, the lattice parameters decrease with increasing Eu concentration because the ionic radius of Eu^{2+} [1.30 Å for coordination number (CN) = 9] is much smaller than that of Ba^{2+} (1.47 Å for CN = 9).[30] Because the incorporation of $(SiN)^+$ makes just a very small red shift (~7 nm) of the host lattice absorption edge (Fig. 7), the broad absorption bands superimposed on the absorption curve of the host lattice can be readily assigned to the Eu^{2+} ions in the spectral range of 300–500 nm. With the Eu content increasing from 1 to 10 mol %, the absorption edge of Eu^{2+} extends from 400 to 460 nm; meanwhile, its absorption intensity becomes intense (Fig. 7). Clearly, the principal excitation band shifts to longer wavelength (i.e., 400–440 nm) at high Eu concentration (Fig. 8), in agreement with the reflection spectra (Fig. 7). This can be understood from shrinkage of the lattice (Fig. 6), which induces a larger crystal field splitting. Excitation in the range of 400–440 nm yields a green emission with a maximum at about 500–526 nm, depending on the Eu content. The red shift of the emsission band is attributed to a larger crystal-field splitting (i.e., 8600 vs 12,000 cm^{-1} for 1 and 10% Eu, respectively), originating from shortening of the Ba_{Eu}–O/N bond in combination with an increase of the Stokes shift (e.g., 2800 vs 3700 cm^{-1} for 1 and 10% Eu, respectively). For long excitation wavelength (440 nm) the in-

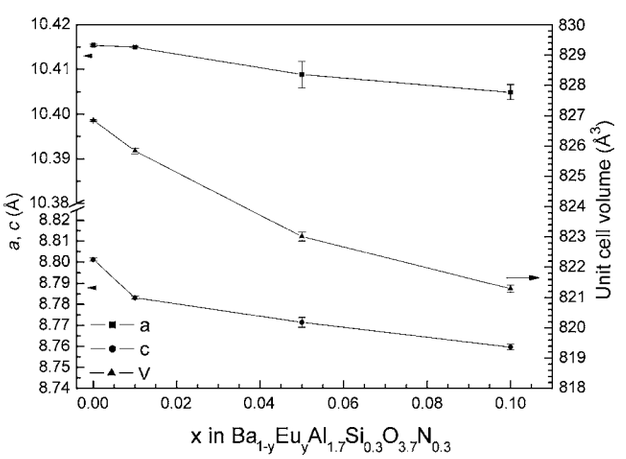

Figure 6. Relationship between the lattice parameters of $Ba_{1-y}Eu_yAl_{1.7}Si_{0.3}O_{3.7}N_{0.3}$ and the Eu concentration.

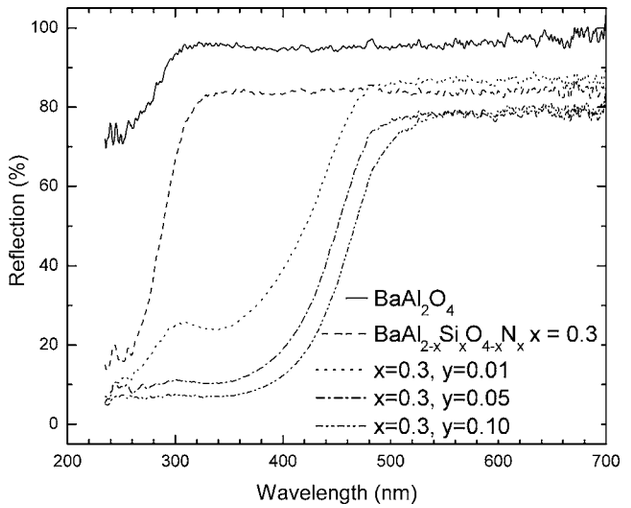

Figure 7. Reflection spectra of $BaAl_{2-x}Si_xO_{4-x}N_x$ ($x = 0$, 0.3) and $Ba_{1-y}Eu_yAl_{2-x}Si_xO_{4-x}N_x:Eu^{2+}$ ($x = 0.3$, $y = 0.01$, 0.05, 0.10 corresponding to 1, 5, and 10 mol % Eu).

tegrated emission intensity increases for higher Eu contents whereas it decreases for short excitation wavelength (390 nm) (see inset in Fig. 8).

Conclusions

The maximum solubility of $(SiN)^+$ in $MAl_{2-x}Si_xO_{4-x}N_x$ with tridymite structure significantly decreases from Ba to Sr and Ca compounds. In $CaAl_2O_4$ and $SrAl_2O_4$, the solubility of $(SiN)^+$ is very limited [i.e., $x \approx 0.025$ (1.25%) and $x \approx 0.045$ (2.25%), respectively], whereas the maximum solubility of $(SiN)^+$ in $BaAl_2O_4$ lattice is about $x \approx 0.6$ (i.e., 30 mol %). As a consequence, the Eu^{2+} emission is found at 440 and 515 nm for Eu-doped $MAl_{2-x}Si_xO_{4-x}N_x$ (M = Ca, Sr), similar to the corresponding compounds without incorporation of nitrogen. $BaAl_{2-x}Si_xO_{4-x}N_x:Eu^{2+}$ exhibits a long-wavelength excitation band peaking at about 440 nm, corresponding to a green emission at about 500–526 nm ($x \approx 0.3$). Compared with $BaAl_2O_4:Eu^{2+}$ (excitation at about 388 nm and emission at about 500 nm), the red shift due to the incorporation of nitrogen can be understood from increased covalency and crystal field splitting. The luminescence properties of $BaAl_{2-x}Si_xO_{4-x}N_x:Eu^{2+}$ can be further modified by adjusting the amount of $(SiN)^+$ and Eu concentration. Consequently, $BaAl_{2-x}Si_xO_{4-x}N_x:Eu^{2+}$ shows high potential as a green-emitting conversion phosphor for white-light LED applications.

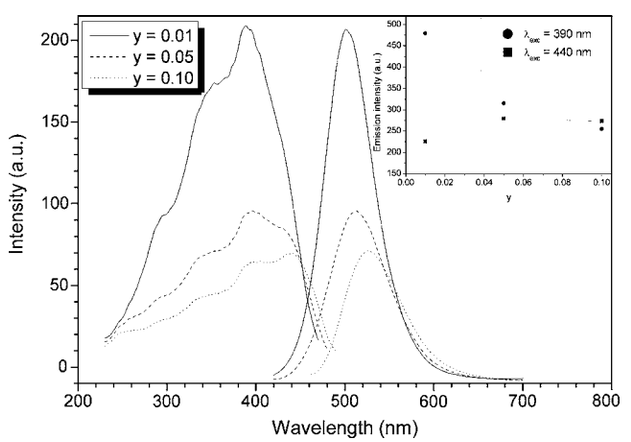

Figure 8. Excitation (left) and emission (right) spectra dependence of x in $Ba_{1-y}Eu_yAl_{1.7}Si_{0.3}O_{3.7}N_{0.3}$ ($\lambda_{exc} = 390$ nm, $\lambda_{em} = 500$ nm for $x = 0.01$; $\lambda_{exc} = 440$ nm, $\lambda_{em} = 515$ nm for $x = 0.05$; and $\lambda_{exc} = 440$ nm, $\lambda_{em} = 530$ nm for $x = 0.10$). Inset shows the integrated emission intensity as a function of the Eu concentration ($\lambda_{exc} = 390$ nm and $\lambda_{exc} = 440$ nm).

Eindhoven University assisted in meeting the publication costs of this article.

References

1. G. Blasse and B. C. Grabmaier, *Luminescent Materials*, Springer-Verlag, Berlin (1994).
2. F. C. Palilla, A. K. Levine, and M. R. Tomkus, *J. Electrochem. Soc.*, **115**, 642 (1968).
3. V. Abbruscato, *J. Electrochem. Soc.*, **118**, 930 (1971).
4. S. Tanaka, I. Ozaki, T. Kunimoto, K. Ohmi, and H. Kobayashi, *J. Lumin.*, **87**, 1250 (2000).
5. H. Yamamoto and T. Matsuzawa, *J. Lumin.*, **727**, 287 (1997).
6. W. Horkner and H. K. Müller-Buschbaum, *J. Inorg. Nucl. Chem.*, **38**, 983 (1976).
7. A. R. Schulze and H. K. Müller-Buschbaum, *Z. Anorg. Allg. Chem.*, **475**, 205 (1981).
8. W. Horkner and H. K. Müller-Buschbaum, *Z. Anorg. Allg. Chem.*, **451**, 40 (1979).
9. G. Blasse and A. Bril, *Philips Tech. Rev.*, **31**, 304 (1970).
10. J. Hölsa, H. Jungner, M. Lastusaari, and J. Niittykoski, *J. Alloys Compd.*, **326**, 323 (2001).
11. T. Aitasalo, J. Holas, H. Jungner, J. C. Krupa, M. Lahtinen, M. Lastusaari, J. Legendziewica, J. Niittykoski, and J. Valkonen, *Radiat. Eff. Defects Solids*, **158**, 309 (2003).
12. J. Niittykoski, T. Aitasalo, J. Holas, H. Jungner, M. Lastusaari, M. Parkkinen, and M. Tukia, *J. Alloys Compd.*, **374**, 108 (2004).
13. S. H. Ju, U. S. Oh, J. C. Choi, H. L. Park, T. W. Kin, and C. D. Kim, *Mater. Res. Bull.*, **35**, 1831 (2000).
14. D. Ravichandran, S. T. Johnson, S. Erdei, R. Roy, and W. B. White, *Displays*, **18**, 197 (1999).
15. T. Matsuzawa, Y. Aoki, N. Takeuchi, and Y. Murayama, *J. Electrochem. Soc.*, **143**, 2670 (1996).
16. *Light Emitting Diodes (LEDs) for General Illumination Update 2002*, J. Y. Taso, Editor, Optoelectronics Industry Development Association, Washington, DC (2002).
17. J. W. H. van Krevel, Ph.D. Thesis, Eindhoven University of Technology, Eindhoven, The Netherlands (2000).
18. H. A. Höppe, H. Lutz, P. Morys, W. Schnick, and A. Seilmeier, *J. Phys. Chem. Solids*, **2001**, 61 (2000).
19. J. W. H. van Krevel, J. W. T. van Rutten, H. Mandal, H. T. Hintzen, and R. Metselaar, *J. Solid State Chem.*, **165**, 19 (2002).
20. S. Hampshire, H. K. Park, and D. P. Thompson, *Nature (London)*, **274**, 880 (1978).
21. J. W. H. van Krevel, H. T. Hintzen, and R. Metselaar, *Mater. Res. Bull.*, **35**, 747 (2000).
22. H. T. Hintzen and Y. Q. Li, Pat. WO 2004/029177 A1 (2004).
23. H. M. Rietveld, *J. Appl. Crystallogr.*, **2**, 65 (1969).
24. A. C. Larson and R. B. Von Dreele, Report LAUR 86-748, Los Alamos National Laboratory, Los Alamos, NM (2000).
25. B. H. Toby, *J. Appl. Crystallogr.*, **34**, 210 (2001).
26. W. Schnick and H. Huppertz, *Chem.-Eur. J.*, **3**, 679 (1997).
27. K. H. Jack, *J. Mater. Sci.*, **11**, 1135 (1976).
28. K. H. Jack, in *Progress in Nitrogen Ceramics*, F. L. Riley, Editor, p. 45, Martinus Nijhoff Publishers, Boston (1983).
29. W. Schnick, *Int. J. Inorg. Mater.*, **1267**, 3 (2001).
30. R. D. Shannon, *Acta Crystallogr., Sect. A: Cryst. Phys., Diffr., Theor. Gen. Crystallogr.*, **32**, 751 (1976).